Pramana – J. Phys. (2016) 87: 30
DOI 10.1007/s12043-016-1237-3

Structural, photoconductive, thermoelectric and activation energy measurements of V-doped transparent conductive SnO_2 films fabricated by spray pyrolysis technique

R NASIRAEI, M R FADAVIESLAM* and H AZIMI-JUYBARI

School of Physics, Damghan University, Damghan, Iran
*Corresponding author. E-mail: m.r.fadavieslam@du.ac.ir

MS received 29 January 2015; revised 25 October 2015; accepted 18 November 2015; published online 21 July 2016

Abstract. This report investigated the structural, optical and electrical properties of V-doped SnO_2 thin films deposited using spray pyrolysis technique. The SnO_2:V films, with different V-content, were deposited on glass substrates at a substrate temperature of 550°C using an aqueous ethanol solution consisting of tin and vanadium chloride. X-ray diffraction studies showed that the SnO_2:V films were polycrystalline only with tin oxide phases and the preferred orientations are along (1 1 0), (1 0 1), (2 1 1) and (3 0 1) planes. Using Scherrer formula, the grain sizes were estimated to be within the range of 25–36 nm. The variation in sheet resistance and optical direct band gap are functions of vanadium doping concentration. Field emission scanning electron microscopy (FESEM) revealed the surface morphology to be very smooth, yet grainy in nature. Optical transmittance spectra of the films showed high transparency of about ∼69–90% in the visible region, decreasing with increase in V-doping. The direct band gap for undoped SnO_2 films was found to be 3.53 eV, while for higher V-doped films it shifted toward lower energies in the range of 3.27–3.53 eV and then increased again to 3.5 eV. The Hall effect and Seebeck studies revealed that the films exhibit n-type conductivity. The thermal activation energy, Seebeck coefficient and maximum of photosensitivity in the films were found to be in the range of 0.02–0.82 eV (in the low-temperature range), 0.15–0.18 mV K^{-1} (at $T = 350$ K) and 0.96–2.84, respectively.

Keywords. Thin film; spray pyrolysis; SnO_2:V.

PACS No. 68.55.–a

1. Introduction

Tin oxide (SnO_2) is one of the most interesting transparent conducting oxides (TCO). It has high optical transparency in the visible region (∼400–800 nm) of the electromagnetic spectrum with high electrical conductivity. SnO_2 nanostructures are wide band gap n-type semiconductor materials (3.6–3.8 eV) [1–9]. They can be used as transparent conductors [10–13], dye-sensitized solar cells [1–4], gas sensors [1,3,6], optoelectronic devices [2,4], flat-panel displays [2–4], light-emitting diodes (LED) [2,8,9], electrochromic devices [11,14], electromagnetic shielding [14], functional glasses [14], architectural windows [15], smart windows [15], photovoltaic films [15], polymer-based electronics [15], liquid crystal displays [10,16], heat mirrors [10,12], antifoggy windows [17], touch screens [2,11,16], transistors [9,13], low emissivity windows [9], window defrosters [9], semiconductor lasers [9] and plasma panel displays [16]. For these applications, TCOs must have wide band gap (>3 eV), high carrier density ($\geq 10^{20}$ cm^{-3}), good electrical conductivity ($\rho \leq 10^{-3}$ Ω cm) and high Hall mobility ($\geq$62.5 cm^2/Vs) [2]. However, pure SnO_2 usually needs modifications in terms of additive incorporation to modify its conductivity and optical absorption. The stoichiometric SnO_2 has low optical and electrical performance because of its low intrinsic carrier density and mobility. Doping with fluorine (F), indium (In), antimony (Sb) and vanadium (V) improve its optical properties and conductivity [15]. Regarding atomic radius of Sn^{4+} (0.71 Å) and V^{3+} (0.74 Å), substitution of V^{3+} or V^{5+} ions in lattice positions of Sn^{4+} is possible. A variety of techniques, such as chemical vapour deposition [18–21], dip coating [8,22], spray pyrolysis [13–16], sol–gel method [23,24],

sputtering [20,25], evaporation [10], pulsed laser deposition [9,12], thermal evaporation [1], hydrothermal method and spin-coating [2], electron beam evaporation [17] and photochemical method [6] are used for the preparation of SnO_2 thin films.

The present study investigated the characteristics of V-doped SnO_2 thin films prepared by spray pyrolysis technique. For this purpose, at the first step, spray pyrolysis deposition technique was used for the preparation of SnO_2:V thin films. This technique was simple, cheap and easily adaptable for large area deposition compared to other techniques. Then, structural, electrical, optical and thermoelectrical properties of the deposited films were studied and discussed. Magnetic property of SnO_2:V films is not studied in this work. The structural, electrical and optical properties of the thin films were examined in relation to the increase in the vanadium amount.

2. Experimental procedure

2.1 *Deposition of V-doped SnO_2 thin films by the spray pyrolysis technique*

The V-doped SnO_2 thin films were deposited on glass substrates using a typical spray pyrolysis coating technique [26]. The precursor solution was prepared by dissolving 0.075 M stannic chloride ($SnCl_4{:}5H_2O$) and different amounts of vanadium chloride (VCl_3) in 20 ml of solvent, a mixture of double distilled water and ethanol, in a volume ratio of 1:1. To increase the solubility of stannic chloride, a few drops of HCl was also added to the solution [14]. The atomic ratio of [V]/[Sn] in the solution was changed from 0 to 10 at%. Before the preparation of films, glass substrates were cleaned and placed on the hot plate and the undoped and V-doped SnO_2 films were deposited on rotating hot substrates under the conditions mentioned in table 1. To prevent a rapid reduction in the temperature of the hot plate, spraying was done in short time intervals. All experiments were done under approximately similar conditions.

2.2 *Structural and optical characterization of films*

X-ray diffraction (XRD) patterns of V-doped SnO_2 thin films were recorded by a D8 Advanced Bruker system using Cu K_α ($\lambda = 0.154056$ nm) radiation with 2θ in 10–70° range. The average crystalline grain size was calculated using Scherrer's formula based on the XRD patterns [26]:

$$D = \frac{K\lambda}{\delta w \cos\theta}, \tag{1}$$

Table 1. Spray deposition parameters for the preparation of SnO_2:V films.

Spray solution volume (ml)	20
Carrier-gas pressure (atm)	3
Spray deposition rate (ml/min)	10
Nozzle to substrate distance (cm)	40
Spray nozzle diameter (atomizer) (mm)	0.2
Hot plate rotation speed (rpm)	60
Substrate temperature (°C)	550

where D is the average crystalline (grain) size, K is a constant ($\sim$1), λ is the X-ray wavelength, δw is the full-width at half-maximum (FWHM) of the XRD peaks and θ is the Bragg angle.

The surface morphology of the films was studied using field emission scanning electron microscopy (FESEM) using a HITACHI S4160 system and atomic force microscopy (AFM). The optical absorption and transparency of the films were measured in the wavelength range of 300–1100 nm using a Unico 4802 UV–Vis double beam spectrophotometer at room temperature. The thickness (t) of the films was determined by using the Swanepoel method [27]. The direct optical band gap energy (E_g) for V-doped SnO_2 thin films was obtained by optical absorption measurements and by plotting $(\alpha h\nu)^2$ vs. photon energy ($h\nu$) and using the following relation [14]:

$$(\alpha h\nu)^2 = A(h\nu - E_g), \tag{2}$$

where α is the absorption coefficient and A and E_g are a constant and the direct band gap energy of the material, respectively.

2.3 *Photoconductive, thermoelectric and activation energy measurements*

For measuring the photoconductivity and the thermoelectric electromotive force (EMF) of the films, the two ends of the samples were coated with aluminum by thermal evaporation in vacuum. The electrical resistivity of V-doped SnO_2 thin films on a non-conducting glass slide was determined by the DC two-probe method and dark conductivity was calculated for all the samples.

The photosensitivity in these films is defined as [28]

$$S = \frac{R_l - R_d}{R_d}, \tag{3}$$

where R_l and R_d are the electrical resistance in light (6000 lux) and in the dark, respectively. All the samples were illuminated from a normal light source (300 W)

at distance $d = 20$ cm for 600 s before recording R_1. The electrical resistance of the thin films was measured by UNI-T multimeters and the light intensity was measured by a TES-1339 light meter.

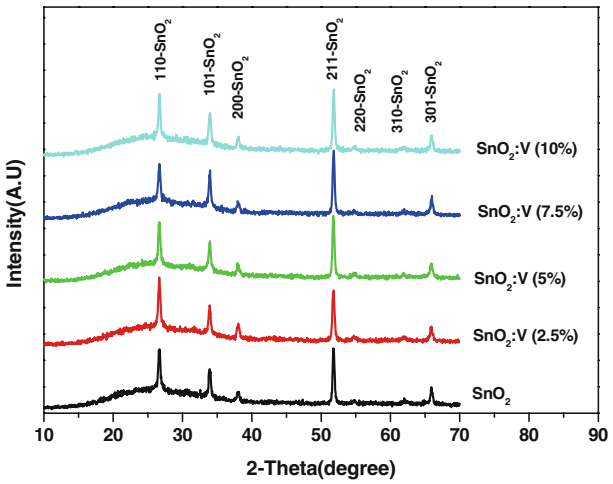

Figure 1. XRD patterns of SnO_2:V thin films for different doping levels.

The thermoelectric EMF of the V-doped SnO_2 was measured by applying a temperature gradient between the two ends of the samples at the temperature range of 300–500 K [29]. An electric heater with an electrical power of 300 W for heating one side (hot side) and an ice water bath for cooling the other side (cold side) were used. A schematic view of the apparatus is shown in ref. [26]. The open circuit thermovoltage generated by the sample was measured using a digital microvoltmeter.

The temperature difference between the two ends of the sample causes the transport of carriers from the hot to the cold end, thus creating an electric field, which gives rise to thermovoltage across the ends. The thermovoltage generated is directly proportional to the temperature gradient applied to the two ends of the semiconductor thin films. From the sign of the potentiometer terminals connected to the two ends of the sample, the sign of charge carriers is obtained. In this measurement, the negative and positive terminals were connected to the hot and cold ends, respectively. Therefore, the films show n- or p-type conductivity.

Table 2. XRD analysis results for four main peaks of 1 1 0, 1 0 1, 2 1 1 and 3 0 1 in V-doped SnO_2 films (all films have tetragonal structure).

Sample name	2θ (°)	d (Å)	$h\,k\,l$	Intensity (Cps)	Grain size (nm)	FWHM (°)
SnO_2:V(0 at%)	26.654	3.34	1 1 0	98.9	32	0.372
SnO_2:V(0 at%)	33.881	2.64	1 0 1	67.9	25	0.367
SnO_2:V(0 at%)	51.792	1.76	2 1 1	100	30	0.328
SnO_2:V(0 at%)	65.882	1.42	3 0 1	40.1	31	0.338
SnO_2:V(2.5 at%)	26.658	3.34	1 1 0	100	33	0.36
SnO_2:V(2.5 at%)	33.91	2.64	1 0 1	61.4	27	0.337
SnO_2:V(2.5 at%)	51.767	1.76	2 1 1	82.4	26	0.374
SnO_2:V(2.5 at%)	65.883	1.42	3 0 1	31.9	26	0.403
SnO_2:V(5 at%)	26.645	3.34	1 1 0	91.5	36	0.334
SnO_2:V(5 at%)	33.929	2.64	1 0 1	64.3	26	0.351
SnO_2:V(5 at%)	51.785	1.76	2 1 1	100	29	0.348
SnO_2:V(5 at%)	65.931	1.42	3 0 1	32.9	25	0.42
SnO_2:V(7.5 at%)	26.666	3.34023	1 1 0	81.7	32	0.375
SnO_2:V(7.5 at%)	33.953	2.63823	1 0 1	73	27	0.345
SnO_2:V(7.5 at%)	51.822	1.76279	2 1 1	100	31	0.323
SnO_2:V(7.5 at%)	65.95	1.41528	3 0 1	37.8	35	0.305
SnO_2:V(10 at%)	26.677	3.34	1 1 0	93.4	36	0.326
SnO_2:V(10 at%)	33.954	2.64	1 0 1	66.6	25	0.375
SnO_2:V(10 at%)	51.816	1.76	2 1 1	100	30	0.328
SnO_2:V(10 at%)	65.922	1.42	3 0 1	34.6	28	0.372

According to the Seebeck effect [30], the thermoelectric power (TEP) is calculated using

$$\varepsilon = \alpha \Delta T + \frac{b}{2}(\Delta T)^2 + \cdots, \tag{4}$$

where ε is the EMF, α is the TEP (Seebeck coefficient), ΔT is the temperature difference between the edges of the sample and b is a constant. If ΔT is very small, eq. (4) can be written as

$$\varepsilon = \alpha \Delta T. \tag{5}$$

That is, the thermoelectric EMF, ΔV, is proportional to ΔT. The Seebeck coefficients were determined by calculating the slope of the thermoelectric EMF vs. the temperature difference curve.

For determining the activation energy level of V-doped films, the temperature dependence of dark electrical resistance was measured in the temperature range 25–200°C in vacuum with 30 Torr pressure. The data were fitted to the Arrhenius equation [31].

$$R = R_0 \mathrm{e}^{(E_\mathrm{a}/K_\mathrm{B}T)}, \tag{6}$$

where R_0 is a parameter dependent on the sample characteristics (thickness, structure, etc.), E_a denotes the thermal activation energy of electrical resistance and K_B is the Boltzmann constant.

3. Result and discussion

3.1 *Structure properties*

The XRD patterns of SnO_2:V films for 0–10 at% V-doping in film are shown in figure 1. For all the samples, the characteristic diffraction peaks at $2\theta = 26.6°$, 33.9°, 51.8° and 65.9° correspond to the (1 1 0), (1 0 1), (2 1 1) and (3 0 1) planes of a tetragonal rutile structure of the cassiterite SnO_2 phases (space group P42/mnm). The presence of other orientations such as (2 0 0) and (3 1 0) has also been detected, but in considerably lower intensities. By V-doping in film, no lines corresponding to Sn–V–O phases or vanadium oxides were detected. It is also observed from figure 1 that higher V concentration gives good quality films with improved crystallinity as evidenced by intense diffraction peaks. Regarding atomic radius of Sn^{4+} (0.71 Å), V^{3+} (0.64 Å) and V^{5+} (0.54 Å), in doping levels, substitution of V^{3+} or V^{5+} ions in lattice positions of Sn^{4+} is possible and clearly evident. The XRD analysis results for four main peaks at (1 1 0), (1 0 1), (2 1 1) and (3 0 1) planes, grains size and the crystallographic characteristics of the SnO_2:V films, are presented in table 2. As seen, the

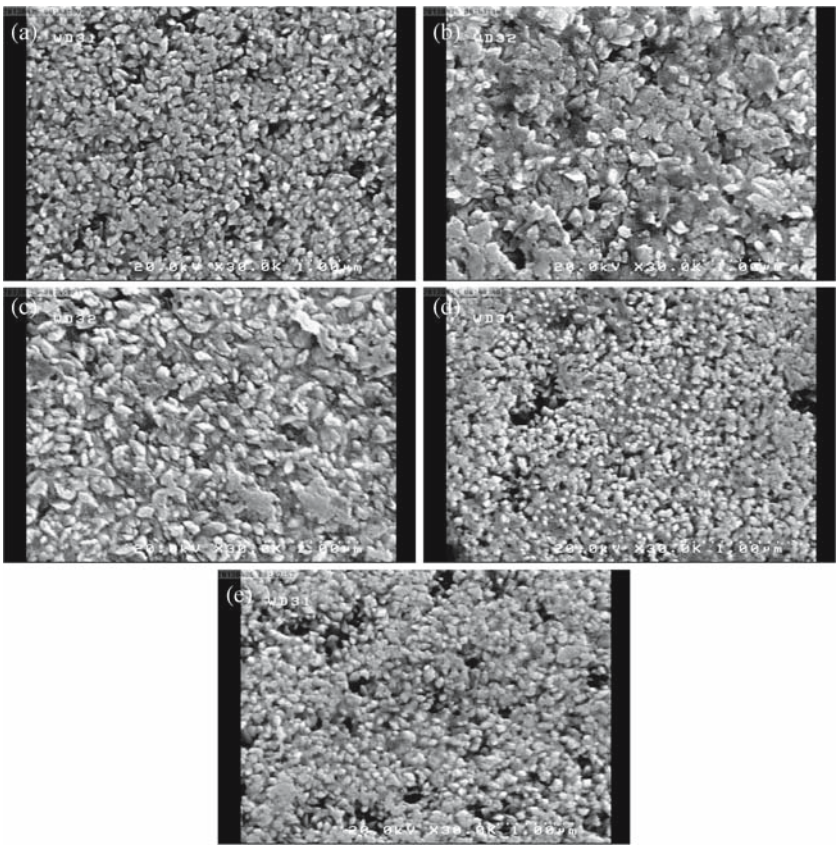

Figure 2. FESEM images of SnO_2:V films for different V-content: (**a**) 0, (**b**) 2.5, (**c**) 5, (**d**) 7.5 and (**e**) 10 at%.

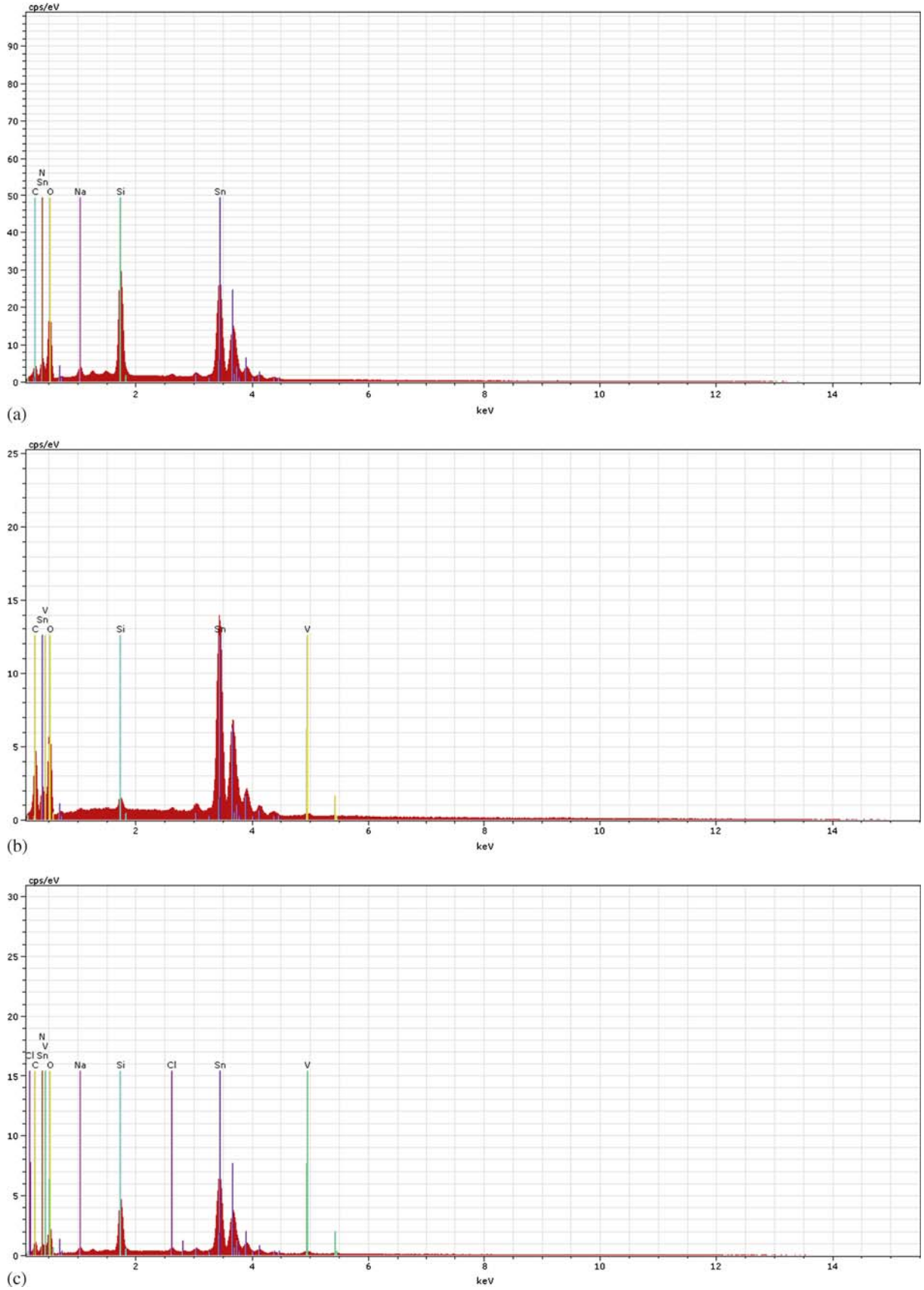

Figure 3. Energy-dispersive X-ray analysis spectra of pure and V-doped SnO_2 thin films: (**a**) undoped SnO_2, (**b**) 5% V-doped SnO_2 and (**c**) 10% V-doped SnO_2.

grain sizes in various orientations are in the range of 25–36 nm.

Figure 2 shows the comparative morphology of pure and vanadium-doped tin oxide films. Both doped and undoped films deposited, showed nearly similar morphology and the grains can be clearly seen. It was observed that the surface morphologies of the films were dependent upon the doping concentration. Based on the observations, particle size decreased with the increase in V-doping. In high doping levels, particles tend to form smaller clusters. It was seen that the grains exhibit average sizes of 47, 43, 45, 41 and 38 nm for V-doping from 0, 2.5, 5, 7.5 and 10 at% in film, respectively. The grain sizes of FESEM images are larger than that predicted by Scherrer's formula from the XRD spectra. Obviously, each particle of the SEM image contains many single-crystal grains.

The element analysis in the films is done using EDX measurement. The EDX spectra plotted in figure 3 indicate the existence of Sn, O and V inside the films. These results show that the atomic ratios in the spray solutions are higher than that in deposited films.

The surface morphology of the films was studied by atomic force microscopy (AFM). The AFM scans of (a) undoped, (b) 5 at% and (c) 10 at% V-doped SnO_2 films are shown in figure 4. The RMS roughnesses were about 36.8, 34.7 and 30 nm for undoped, 5 at% and 10 at% V-doped SnO_2 films respectively. This indicates that film roughness is significantly affected by vanadium doping.

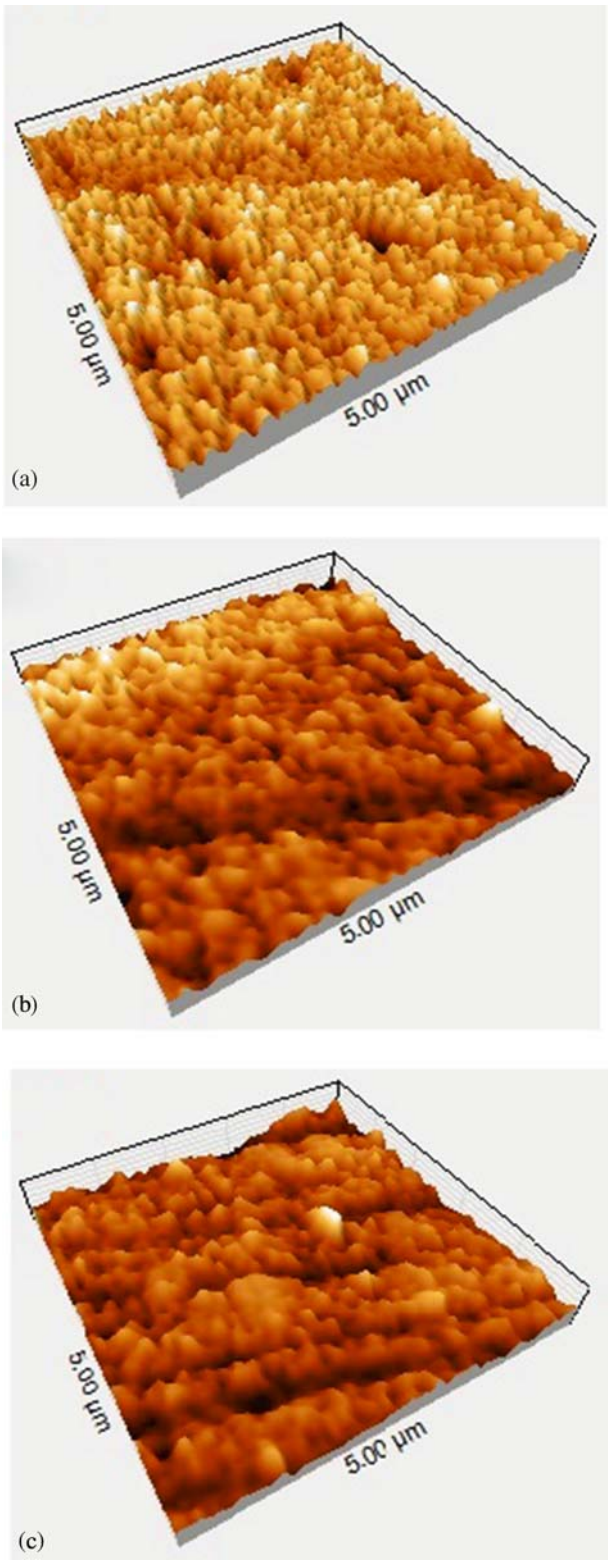

Figure 4. AFM images of SnO_2:V films for different V-content: (**a**) 0, (**b**) 5 and (**c**) 10 at%.

3.2 *Optical properties*

From the optical transmission spectra shown in figure 5, it can be seen that transparency in the visible region (420–800 nm) is about ∼69–90%. The transparency of pure SnO_2 film is 90% and the other films are in the range of 69–78%. Therefore, transparency

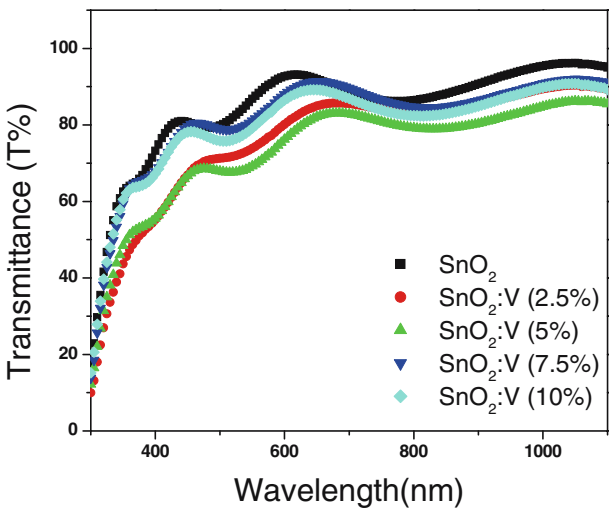

Figure 5. The variation of transmittance with the wavelength of SnO_2:V thin films for different doping levels.

decreases with increase in V-content due to presence of impurity and disorder in SnO_2 lattice.

Figure 6 displays the dependence of the optical direct band gap energy (E_g) on V-doping level. The direct band gap values range from 3.53 to 3.27 eV, which decreases with increase in V-content. The fluctuation of optical band gap with V-doping can be explained as (i) first, the decrease in E_g values of undoped SnO_2 and upto 2.5 at% V-doped SnO_2 may be attributed to the increase in nanograin size in films structure [32]; (ii) secondly, increase in E_g values of SnO_2 in 5–7.5 at% V-doping may result from decrease in the nanograin size of particles [33]. In addition, change in energy gap from 3.31 to 3.5 eV may be due to decrease in grain size in high doping levels [8].

3.3 *Electrical properties*

The results of the electrical resistivity, the photoconductivity, thermoelectrical and Hall effect measurements of thin films are summarized in table 3. The variation in sheet resistance and carrier concentration of SnO_2:V films is plotted in figure 7, as a function of vanadium doping concentration. The variation in sheet resistance and optical direct band gap of SnO_2:V films is plotted in figure 8, as a function of vanadium doping concentration. It shows the dependency between the variation in sheet resistance and optical direct band gap as a function of vanadium doping concentration. The electric conductivity, besides the electronic charge distribution, is strongly dependent on the scattering phenomena related to the size, for instance, the grain size and the size of the film and the scattering from impurities. Hence, we argue that V_2O_3 which has more pronounced phases formed at lower concentrations compared to higher ones, behave as scattering impurities for conduction electrons. It may be seen that the sheet resistance decreases with the increase in vanadium concentration from 0 to 2.5 at% (see figure 6). It was found that the sheet resistance increased for the doping of vanadium above 7.5 at% and then decreased for the doping of vanadium above 10 at%. The variation in the sheet resistance of tin oxide thin films

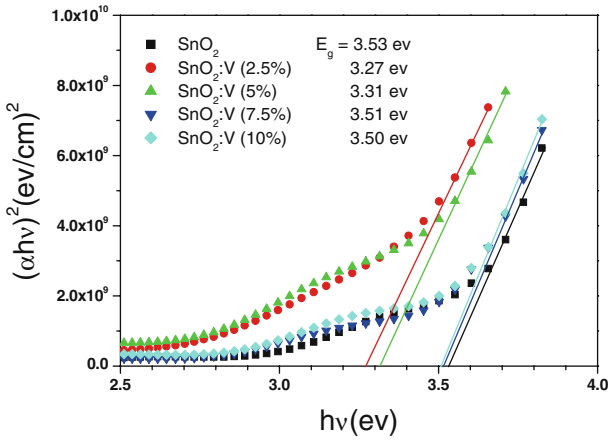

Figure 6. Plots of $(\alpha h\nu)^2$ vs. $(h\nu)$ for SnO_2:V thin films for different doping levels.

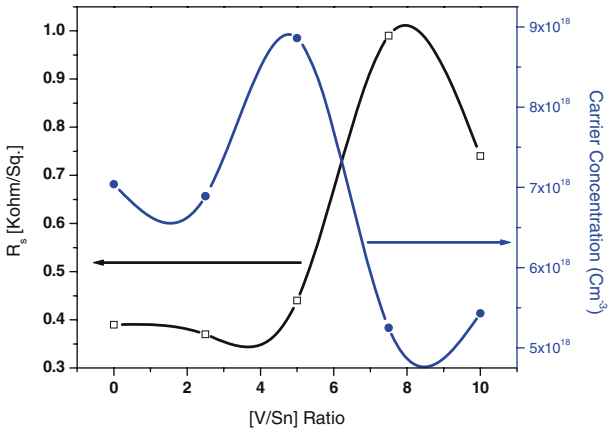

Figure 7. The variation in sheet resistance and carrier concentration of SnO_2:V thin films for different doping level $[V/Sn]$ ratios.

Table 3. The results of electrical, thermopower, Hall effect and photoconductivity measurements for different V-doped SnO_2 films.

Sample $[V/Sn]$	t (nm)	R_s (KΩ/ϒ)	ρ (Ω·cm)	Conductivity type	Carrier concentration (cm^{-3})	Seebeck coefficient ($\mu V\,K^{-1}$) $T = 350$ K	Maximum of photosensitivity S, $\left\lvert\frac{\Delta R}{R}\right\rvert$	E_a (eV) Low-temperature range	E_a (eV) High-temperature range
Undoped	369	0.39	1.54	n	7.04×10^{18}	183	0.96	0.02	0.51
2.5	402	0.37	1.48	n	6.89×10^{18}	158	1.52	0.82	0.35
5	376	0.44	1.65	n	8.86×10^{18}	150	1.86	0.08	0.55
7.5	396	0.99	3.92	n	5.25×10^{18}	175	2.84	0.33	–
10	373	0.74	2.76	n	5.43×10^{18}	167	1.53	0.18	0.72

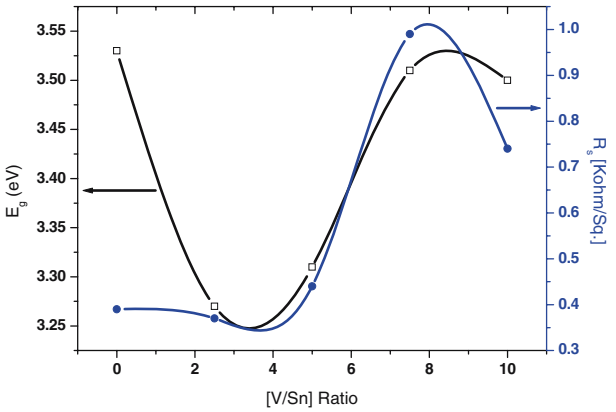

Figure 8. The variation in sheet resistance and optical direct band gap of SnO_2:V thin films for different doping level $\left[V/Sn\right]$ ratios.

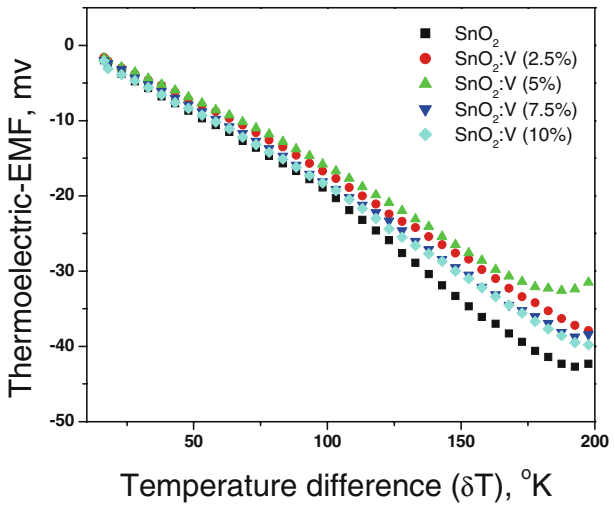

Figure 9. The variation in thermoelectric-EMF with temperature difference of SnO_2:V thin films for different doping levels.

with vanadium doping can be explained on the basis of the presence of V in two oxidation states, V^{5+} and V^{3+}. When SnO_2 is doped with V in the range of 0–2.5 at%, some of the V^{5+} ions in the lattice are replaced by Sn^{4+}, resulting in the generation of free electron, thus reducing the sheet resistance [34]. Another reason for decreasing sheet resistance in this region can be explained by the XRD patterns, which is due to the decrease in amorphous phase and disorders (see figure 1). Also, in this region, X-ray diffraction peak intensity of (1 1 0) plane increases, while peak intensity of (1 0 1), (2 1 1) and (3 0 1) planes decreases. This is caused by migration of Sn^{4+} ions to middle sites as well as substitution of V^{5+} in Sn^{4+} sites. In contrast, in the region with doping levels between 2.5 and 7.5 at% in film, the sheet resistance of the films increases, because of substitution of a part of V^{3+} ions in Sn^{4+} state, resulting in the formation of acceptor states and a concomitant loss of carriers. Also, peak intensity of (1 1 0) plane decreases and amorphous phase increases. In addition, generally when the grain size decreases, as seen in figure 2, the density of grain boundaries in the film increases. Therefore, the scattering of carriers at grain boundaries increases and their mobility increases resulting in an increase in the electrical resistivity of the film [35]. With increase in doping level from 7.5 to 10 at%, the sheet resistance decreases. This circumstance is related to the decreasing atomic disorders in the crystalline structure and the amorphous phase. Also, based on the XRD patterns, intensity of (1 1 0) plane increases. However, the intensities of (1 0 1) and (3 0 1) planes decrease and that of amorphous background decrease.

Measurements of thermoelectrical effect indicate n-type conductivity for thin films (see figure 9). The thermoelectric EMF depends on the location of the Fermi energy in the material, the type of scattering mechanism and the charge the carriers encounter. It increases as the Fermi energy moves further into the energy gap from the bottom edge of the conduction band. This amounts to concluding that the smaller the carrier concentration, the larger the Seebeck coefficient. Thus, a relatively higher thermoelectric EMF for the thin films is due to their higher crystalline and crystallite size. The Seebeck coefficient obtained is as high as $+0.23$ mV/K at $T = 450$ K, for undoped SnO_2 thin film.

The resistance of the investigated thin films decreases with increasing temperature (see figure 10). This indicates that the films have semiconductor-like

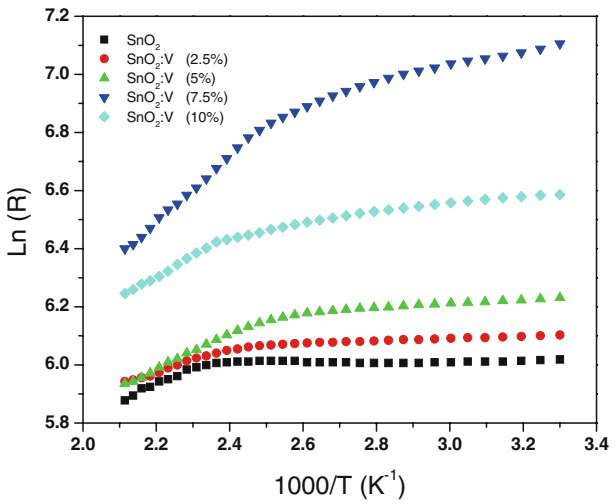

Figure 10. The variation in resistance with temperature of SnO_2:V thin films for different doping levels.

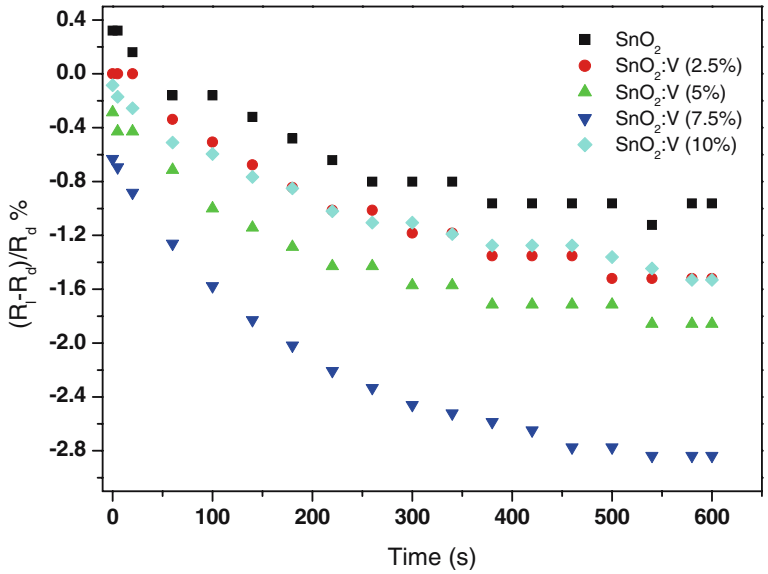

Figure 11. The variation of $S\% = ((R_l - R_d)/R_d) \times 100$ with time of SnO_2:V thin films for different doping levels (at% in solution).

behaviour. The values of activation energy (E_a) evaluated from the slope of the plot of ln R vs. $1000/T$ have been summarized in table 3. Thermal activation energy changed in the range of 0.02–0.82 eV and 0.35–0.72 eV in low-temperature range and high-temperature range, respectively. These activation energies correspond to a shallow donor level and a deep acceptor level [36,37].

The photosensitivity for all the films shows an exponential fall in resistance at first and then a tendency of saturation. The saturation condition is due to a decrease in the rate of photogeneration of carriers related to time. Simultaneously, the recombination process has a main role in reducing the photosensitivity. Consequently, a steady state is obtained where the rate of generation of charge carriers is equal to the recombination rate under constant illumination. This phenomenon is responsible for obtaining a nearly flat profile of photosensitivity at the end (see figure 11). A high photosensitivity of 2.84 was shown by films prepared at ([V]/[Sn]) = 7.5.

4. Conclusions

In summary, applying spray pyrolysis technique, thin films of vanadium-doped tin oxide (SnO_2:V) were successfully prepared at a fixed substrate temperature of 550°C; XRD, FESEM, Hall effect measurement and UV–Vis spectrometry characterize structures, surface morphology, electrical and optical properties of the films. The XRD results showed that all n-type conducting films possessed polycrystalline SnO_2 with a tetragonal rutile structure; on the other hand, average grain size estimated from Scherrer's formula was ranging from 25 to 36 nm. FESEM sample studies showed the surface morphology to be very smooth, yet grainy in nature. Optical transmittance spectra of the films showed high transparency, of about ∼69–90%, in the visible region, decreasing with increase in V-doping. The direct band gap for undoped SnO_2 films was found to be 3.53 eV, while for higher V-doped films shifted toward lower energies in the range 3.53–3.27 eV and then increased again to 3.50 eV. In all films, we have obtained resistivities, Seebeck coefficient and carrier concentration in the order of 1.48–3.92 Ω Cm, 0.15–0.18 mV K^{-1} and 5.25–8.86 Cm^{-3}, respectively.

References

[1] Jyh-Ming Wu, *Thin Solid Films* **517**, 1289 (2008)
[2] Ha-Rim An, Chang Yeoul Kim, Sung-Tag Oh and Hyo-Jin Ahn, *Ceram. Int.* **40**, 385 (2014)
[3] R Mariappan, V Ponnuswamy, P Suresh, R Suresh, M Ragavendar and C Sankar, *Mater. Sci. Semiconductor Process.* **16**, 825 (2013)
[4] Min-Seung Choi, Young-Ju Lee, Jung-Dae Kwon, Yongsoo Jeong, Ju-Yun Park, Yong-Cheol Kang, Pung-Keun Song and Dong-Ho Kim, *Curr. Appl. Phys.* **13**, 1589 (2013)
[5] F A Garcés, N Budini, R R Koropecki and R D Arce, *Thin Solid Films* **531**, 172 (2013)
[6] Dengbaoleer Ao and Masaya Ichimura, *J. Non-Crystalline Solids* **358**, 2470 (2012)
[7] Shadia J Ikhmayies and Riyad N Ahmad-Bitar, *Mater. Sci. Semiconductor Process.* **12**, 122 (2009)
[8] Shuai Chen, Xiaoru Zhao, Haiyan Xie, Jinming Liu, Libing Duan, Xiaojun Ba and Jianlin Zhao, *Appl. Surf. Sci.* **258** (2012)

[9] E Chan y Díaza, Juan M Camacho, A Duarte-Moller, R Castro-Rodríguez and P Bartolo-Pérez, *J. Alloys Compounds* **508**, 342 (2010)
[10] Hong-lei Ma, Xiao-Tao Hao, Jin Ma, Ying-Ge Yang, Jie Huang, De-Heng Zhang and Xian-Gang Xu, *Appl. Surf. Sci.* **191**, 313 (2002)
[11] Bon-Ryul Koo and Hyo-JinAhn, *Ceram. Int.* **40**, 4375 (2014)
[12] Shihui Yu, Weifeng Zhang, Linngxia Li, Dan Xu, Helei Dong and Yuxin Jin, *Appl. Surf. Sci.* **286**, 417 (2013)
[13] C Matei Ghimbeu, R C van Landschoot, J Schoonman and M Lumbreras, *J. Eur. Ceram. Soc.* **27**, 207 (2007)
[14] Mohammad-Mehdi Bagheri-Mohagheghi and Mehrdad Shokooh-Saremi, *Physica B* **405**, 4205 (2010)
[15] B Zhang, Y Tian, J X Zhang and W Cai, *Mater. Lett.* **65**, 1204 (2011)
[16] Ming-Fei Chen, Keh-moh Lin and Yu-Sen Ho, *Mater. Sci. Eng. B* **176**, 127 (2011)
[17] Xiudi Xiao, Guoping Dong, Jianda Shao, Hongbo He and Zhengxiu Fan, *Appl. Surf. Sci.* **256**, 1636 (2010)
[18] Te-Hua Fanga and Win-Jin Chang, *Appl. Surf. Sci.* **252**, 1863 (2005)
[19] S Haireche, A Boumeddiene, A Guittoum, A El Hdiy and A Boufelfel, *Mater. Chem. Phys.* **139**, 871 (2013)
[20] Christoph Körber, Péter Ágoston and Andreas Klein, *Sensors and Actuators B: Chemical* **139**, 665 (2009)
[21] K H Gao, T Lin, X D Liu, X H Zhang, X N Li, J Wu, Y F Liu, X F Wang, Y W Chen, B Ni, N Dai and J H Chu, *Solid State Commun.* **157**, 49 (2013)
[22] E A Morais and L V A Scalvi, *J. Eur. Ceram. Soc.* **27**, 3803 (2007)
[23] Sanju Rani, Somnath C Roy, N Karar and M C Bhatnagar, *Solid State Commun.* **141**, 214 (2007)
[24] Marco A L Pinheiro, Tatiane F Pineiz, Evandro A de Morais, Luis V A Scalvi, Margarida J Saeki and Alberto A Cavalheiro, *Thin Solid Films* **517**, 976 (2008)
[25] P C Lansåker, G A Niklasson and C G Granqvist, *Thin Solid Films* **520**, 3688 (2012)
[26] M R Fadavieslam, N Shahtahmasebi, M Rezaee-Roknabadi and M M Bagheri-Mohagheghi, *Phys. Scr.* **84**, 035705 (2011)
[27] J Sánchez-González, A Díaz-Parralejo, A L Ortiz and F Guiberteau, *Appl. Surf. Sci.* **252**, 6013 (2006)
[28] K Bindu and P K Nair, *Semicond. Sci. Technol.* **19**, 1348 (2004)
[29] G S Nolas, J Sharp and H J Goldsmid, *Thermoelectric basic principles and new materials development* (Springer, Berlin, 2001)
[30] L Li, L Fang, X M Chen, J Liu, F F Yang, Q J Li, G B Liu and S J Feng, *Physica E* **41**, 169 (2008)
[31] E Guneri, C Ulutas, F Kirmizigul, G Altindemir, F Gode and C Gumus, *Appl. Surf. Sci.* **257**, 1189 (2010)
[32] S Marikkannu, M Kashif, N Sethupathy, V S Vidhya, Shakkthivel Piraman, A Ayeshamariam, M Bououdina, Naser M Ahmed and M Jayachandran, *Mater. Sci. Semicond. Process.* **27**, 562 (2014)
[33] E Mokaripoor and M-M Bagheri-Mohagheghi, *Mater. Sci. Semicond. Process* **30**, 400 (2015)
[34] Hiroshi Chiba, Tatsuya Mori, Shuhei Okuda and Katsuyoshi Washio, *Thin Solid Films* **557**, 203 (2014)
[35] R Swapna and M C Santhosh Kumar, *Ceram. Int.* **38**, 3875 (2012)
[36] N Koteeswara Reddy and K T Ramakrishna Reddy, *Physica B Condens. Matter* **368**, 25 (2005)
[37] B Subramanian, C Sanjeeviraja and M Jayachandran, *Mater. Chem. Phys.* **71**, 40 (2001)